Effect of Signal Quantization on Robust Anti-jamming in Snapshot Receivers

Helena Calatrava, *Northeastern University, Boston, MA*
Adrià Gusi-Amigó, *Albora Technologies, London, UK*
Floor Melman, *European Space Agency, Noordwijk, The Netherlands*
Pau Closas, *Northeastern University, Boston, MA*

BIOGRAPHY

Helena Calatrava received her BS and MS in Electrical Engineering from the Universitat Politècnica de Catalunya in 2020 and 2022, respectively. She is currently pursuing a PhD in Electrical Engineering at Northeastern University, Boston. During 2020-2022 she was an intern at Albora Technologies. Her research focuses on GNSS signal processing, remote sensing, target tracking and machine learning.

Adrià Gusi-Amigó is the Head of the GNSS team at Albora Technologies, located in Barcelona, Spain. He earned his MS in Electrical Engineering from the Universitat Politècnica de Catalunya in 2010, followed by a PhD in Electrical Engineering from the Université catholique de Louvain in 2015. His primary research focuses on signal processing for ranging and positioning, as well as multiuser and multipath interference. Additionally, he specializes in the analysis of estimation lower bounds.

Floor Melman received his MS in Aerospace Engineering in 2018 from the Delft University of Technology. During 2018-2020, he worked as a Young Graduate Trainee (YGT) in the navigation directorate on Galileo signals and receivers. Since 2020, he works as a Radio Navigation Engineer at ESA/ESTEC. His main areas of work include PNT algorithms (in harsh environments) and GNSS signal processing.

Pau Closas is an Associate Professor at Northeastern University, Boston, MA. He received the MS and PhD degrees in Electrical Engineering from UPC in 2003 and 2009. He also holds a MS in Advanced Mathematics from UPC, 2014. His primary areas of interest include statistical signal processing, robust stochastic filtering, and machine learning, with applications to positioning systems and wireless communications. He is the recipient of multiple awards including the 2014 EURASIP Best PhD Thesis Award, the 9th Duran Farell Award, the 2016 ION Early Achievements Award, 2019 NSF CAREER Award, and 2022 IEEE AESS Harry R. Mimno Award.

ABSTRACT

GNSS jamming signals are L-band spectrum interferences that can jeopardize the operation of GNSS-based services. Consequently, jamming cancellation and mitigation techniques have received substantial interest in the field of GNSS positioning in the last few years. An advantageous approach to performing jamming mitigation relies on the use of robust statistics, with a framework known as Robust Interference Migration (RIM). In this paper, the RIM methodology is assessed in the context of a GNSS software snapshot receiver architecture under the presence of three jamming interferences simulated as representative cases of common mass-market jammers. A study on the effect of signal quantization in GNSS snapshot receivers is provided with a focus on interference mitigation. Results suggest that the clipping effect originated by the finite quantization dynamic range causes signal distortion, which leads to undesirable receiver performance for a low number of quantization bits. However, when applying RIM, a gain proportional to the number of quantization bits is observed in terms of the number of visible satellite vehicles, availability of the position, velocity and time (PVT) solution, and observed carrier-to-noise density ratio.

I. INTRODUCTION

The growth rate of jamming sources in the last few years has attracted special attention in the GNSS community (Morales Ferre et al., 2020), given that these L-band spectrum interferences can strongly jeopardize the operation of GNSS-based services. Not only a wide variety of jammers is available in the online market (Garcia-Molina and Crisci, 2016), but also signals do not need to be intentional to have a jamming effect on receiver equipment. Some examples of legitimate waveforms that can pose a thread are continuous wave (CW) interferences produced by damaged electronics and signals emitted by the distance measuring equipment (DME) and tactical air navigation (TACAN) aiding systems near L5/E5a (Pullen and Gao, 2012). However, the most common motivation when using a jamming device is user privacy, aiming to prevent the tracking of people and vehicles (Medina et al., 2019a). The overcrowded radio frequency spectrum also enters into the picture with signal harmonics from other wireless systems being present in the GNSS frequency bands (Gao et al., 2016). As satellites are about 20,000 km above the Earth's

surface, propagation losses in the GNSS signal of interest are very high. On the other hand, jammers are placed either on Earth or, in the case of drone jammers, in the proximity of its surface (Morales Ferre et al., 2019), and consequently jamming signals are received with remarkably higher power than the useful GNSS signal. This causes the disruption of receiver performance in areas with radii of several kilometers (Borio et al., 2016; Mitch et al., 2011).

GNSS snapshot receivers are able to operate with much less power consumption than conventional receivers, providing an instantaneous position fix from GNSS digitized signal captured over only a few milliseconds (Fernández-Hernández and Borre, 2016). Their open-loop architecture requires external assistance and the modification of the navigation filter for the computation of a position, velocity and time (PVT) solution (Liu et al., 2020; Linty, 2015). Since navigation messages are not decoded, the signal transmission time needs to be estimated by the receiver. This typically reduces the position solution accuracy down to tens of meters (Dumitraschkewitz, 2020), although it was recently demonstrated that snapshot receivers can be used to achieve high-accuracy RTK solutions Liu et al. (2021). GNSS snapshot receivers are suitable for applications with flexible accuracy requirements or with high computing power restrictions, which makes it possible for manufacturers to integrate them into mobile platforms. As snapshot receivers are limited to the processing of narrow data chunks, it is relevant to assess their performance in the context of interference detection and mitigation, which may differ from the one in conventional receivers (Dumitraschkewitz, 2020). Due to the absence of a tracking module, interference mitigation techniques that require the tracking of the jamming signal are not the most suitable option for snapshot architectures.

Jamming cancellation and mitigation techniques have received substantial interest in the field of GNSS positioning (Amin et al., 2016a). Classical jamming mitigation techniques are formulated as an estimation problem where the jamming signal is detected and estimated to enable Interference Cancellation (IC), commonly through a parametric model. This principle consists in reconstructing the radio frequency interference (RFI) and subtracting it from the received signal. In this way, it is possible to work with a clean signal that is close to the one containing useful GNSS data. Adaptive notch filtering (Borio et al., 2012) and pulse blanking (Borio, 2016) are popular mitigation techniques that make use of the IC principle. Kalman filters can also be used to track and reconstruct jamming signals (Mitch et al., 2013). A major drawback of these IC techniques is that they require the detection and estimation of the jammer waveform. Additionally, some techniques only operate properly when the interference is narrowband and its instantaneous frequency varies slowly in time (Borio and Closas, 2017) or can be tracked. Furthermore, when applying waveform-dependent methods, jamming signal classification is required (Morales Ferre et al., 2019; Wu et al., 2023). Multi-antenna systems (Fernández-Prades et al., 2016) and sparse arrays (Amin et al., 2016b) have been proven to provide benefits in the context of jamming mitigation. These can be complementary to the previously mentioned techniques and also with the robust anti-jamming approach described hereafter.

A different approach to performing jamming mitigation emerged with the use of robust statistics (Borio, 2017b), which do not require the characterization of the jammer waveform. Robust mitigation techniques follow a different approach than the ones implementing the IC principle. This branch of statistics makes it possible to discard disrupted samples by treating them as outliers in certain domains (Li et al., 2019). Narrowband interferences can be seen as outliers in the frequency domain and DME-like signals or pulsed interferences can be seen as outliers in the time domain. To understand why robust methods are so powerful, it is necessary to refer to the *breakdown point* concept, which corresponds to the proportion of disrupted samples that a method can handle before computing a wrong result. Non-robust methods have a breakdown point of 0, while robust methods can achieve a breakdown point of 0.5, which is the maximum possible value, meaning that they are resilient to a certain amount of disruption. In Medina et al. (2019b), a comprehensive guide on the implementation of popular robust methods for PVT estimation is provided.

Zero-memory non-linear functions and non-linear correlators based on robust methods are the basis of robust anti-jamming techniques (Borio and Closas, 2017). In Borio et al. (2018), the Robust Interference Mitigation (RIM) algorithm is introduced, providing an analytical and experimental analysis of its performance without considering the snapshot architecture. This robust pre-correlation technique removes outliers from the received signal without the need for interference detection or estimation. It can be applied in several domains (e.g., frequency and time), showing successful results when compared to other state-of-the-art techniques such as the aforementioned notch filtering and pulse blanking.

In this paper, the performance of the frequency domain RIM algorithm in a GNSS software snapshot receiver is assessed with RFI data simulated by following the jamming signal models in Morales Ferre et al. (2019) for single-tone CW, non-pulsed and pulsed chirp interferences. When assessing the performance of RIM in the literature, authors usually assume that the number of bits is enough to allow for the full signal representation. With this paper, we aim to study what happens when this is not the case and also the algorithm is implemented in a snapshot architecture. A study on the effect of signal quantization in GNSS snapshot receivers in the context of interference mitigation is provided.

The remainder of this paper is as follows: Section II formulates the GNSS and jamming signal models; Section III provides a description of the RIM algorithm processing steps, a review of Loss of Efficiency (LoE) results and a proposal for a recursive method for robust variance estimation; Section IV presents the setup used for the conducted experiment; Section V includes the results and discussion; and Section VI concludes the paper.

II. SIGNAL MODEL

The model of a signal collected by a GNSS receiver can be expressed as (Kaplan and Hegarty, 2005)

$$y(t) = \sqrt{2C}d\left(t-\tau_0\right)c\left(t-\tau_0\right)\cos\left(2\pi(f_{\text{RF}}+f_0)t+\phi_0\right)+\eta(t)+i(t), \tag{1}$$

where C is the useful signal power, $\eta(t)$ is the additive white Gaussian noise (AWGN) term and $i(t)$ corresponds to the jamming interference. The navigation message and the pseudo-random code are represented by $d(\cdot)$ and $c(\cdot)$, respectively. As a consequence of the relative dynamic between the satellite and the receiver, there is a Doppler shift f_0 with respect to the signal radio frequency f_{RF}. Also, the communications channel introduces a delay and phase shift denoted as τ_0 and ϕ_0, respectively.

After amplifying, filtering and down-converting the samples $y(t)$ at the receiver, the I/Q baseband samples are generated as

$$y[n] = \sqrt{C}\tilde{d}\left(nT_s-\tau_0\right)\tilde{c}\left(nT_s-\tau_0\right)e^{j2\pi f_0 nT_s+j\phi_0}+\eta[n]+i[n], \tag{2}$$

where $\tilde{\cdot}$ indicates the impact of front-end filtering on the useful signal component, n is the time index and $[\cdot]$ denotes a discrete time sequence sampled at the receiver sampling frequency $f_s = \frac{1}{T_s}$. The signal $y(t)$ has been down-converted to the baseband frequency and consequently the noise component $\eta[n]$ and the interference $i[n]$ are baseband signals. We model $\eta[n]$ as an AWGN with independent and identically (i.i.d.) real and imaginary parts being σ^2 the variance of each part. This variance can be expressed as a function of the receiver bandwidth B_{R_x} and the power spectral density (PSD) of the input noise $\eta(t)$, denoted as N_0, as $\sigma^2 = \frac{1}{2}N_0 B_{R_x}$.

1. Jamming Signals

Received jamming interferences $i[n]$ can assume several waveforms. According to Morales Ferre et al. (2019), jamming signals can be classified into five categories: Class I jammers are CW modulated signals with a bandwidth up to 100 kHz; Class II and III include single-chirp and multi-chirp jammer signals; Class IV are chirp signals with frequency bursts that aim to expand the band of disrupted frequencies; and finally Class V jammers include pulsed and DME-like signals. The instantaneous frequency $f_J(j)$ of chirp jammers consists in a saw-tooth (ST) waveform that sweeps frequencies from f_{min} to f_{max} periodically every T_{sweep} seconds. Sweep periods are commonly around 10 μs and sweep ranges ($\Delta f = f_{\text{max}} - f_{\text{min}}$) can vary within the range of 10-40 MHz (Borio et al., 2013; Mitch et al., 2011).

Several metrics are adopted in the literature to characterize the relationship between jamming and noise signals (Borio et al., 2016). The jammer-to-noise power ratio (J/N) is defined as the ratio between the received jamming power J and the noise power N, while the jammer-to-noise density power ratio (J/N_0) is defined as the ratio between J and N_0. These two ratios are related as

$$\frac{J}{N} = \frac{J}{N_0}\frac{1}{B_{R_x}} = \frac{JT}{N_0}\frac{1}{N_{\text{snap}}} = \frac{A_J^2}{\sigma^2}, \tag{3}$$

where T is the snapshot duration in seconds, A_J is the amplitude of the jamming signal and N_{snap} corresponds to the number of snapshot samples. Another important metric is the carrier-to-noise density ratio (C/N_0), defined as the ratio between the useful signal power C and N_0. A continuous estimation of this metric is given by the receiver, usually in logarithmic units, dB-Hz.

2. Signal Quantization

RFI detection and mitigation techniques usually assume that input data is quantized with a very high number of bits (Díez-García and Camps, 2019), but this is not the case with most GNSS receivers. Two-bit analog-to-digital converters (ADC) are very common in the market. Without the presence of jamming interferences and under suitable conditions, GNSS receivers provide reasonable results with just 1 quantization bit. However, a better resolution is required to be sensitive to the power difference given by interfered samples and consequently, a higher number of bits is required when applying jamming detection or mitigation techniques.

The number of quantization bits and quantization dynamic range can be dynamically changed according to the characteristics of the received signal. Quantization dynamic range is defined as the difference between the largest and the smallest values that a quantized signal can assume. A fixed dynamic range guarantees a proper representation of the expected noise signal. However, samples affected by jamming suffer from clipping because, as the name implies, the range is fixed and it is not susceptible to changes in the received power. This clipping effect occurs when the number of quantization bits is not enough to represent the signal, in cases such as when the signal is overpower by a jammer. In Díez-García and Camps (2019), an adaptive dynamic range system based on automatic gain control (AGC) is proposed, where the quantization thresholds and the dynamic range are determined by the variance of the input snapshot. With a high number of quantization bits, the signal resolution will be high enough to assign several quantization values to non-interfered samples.

In Borio (2008), an expression to compute the quantization values as a function of the number of quantization bits is given. With *B* being the number of quantization bits, the quantized signal can assume the values in the set $B = \{-(2^B - 1), ..., -3, -1, 1, 3, ..., 2^B - 1\}$, which corresponds to the odd numbers $\{2i + 1\}_{i=-2^{B-1},-2^{B-1}+1,...,2^{B-1}-1}$. Quantization thresholds can be computed as $Q_0 = \{-(2^B - 1) + 2, ..., -3, -1, 0, 1, 3, ..., (2^B - 1) - 2\}$. Also, the input signal has to be multiplied by a factor that corresponds to the optimal AGC gain value, which depends on the snapshot variance σ^2. From the expression of quantization loss found in (Borio, 2008), it is possible to extract the optimal value of the AGC optimal gain as a function of the number of quantization bits (see Table 1).

B	1	2	3	4	5	6	7	8
AGC Optimal Gain	-	$\frac{1.005}{\sigma^2}$	$\frac{1.707}{\sigma^2}$	$\frac{2.984}{\sigma^2}$	$\frac{5.316}{\sigma^2}$	$\frac{9.61}{\sigma^2}$	$\frac{17.586}{\sigma^2}$	$\frac{32.508}{\sigma^2}$

Table 1: AGC optimal gain as a function of the number of quantization bits. Values have been derived from the quantization loss expression in (Borio, 2008).

III. ROBUST INTERFERENCE MITIGATION

The RIM algorithm can be implemented in three processing steps: a first linear transform $\mathbf{T}_1$, a Zero-Mean Non-Linearity (ZMNL) and a second linear transform $\mathbf{T}_2$ that inverts the effect of the first one. $\mathbf{T}_1$ transforms the snapshot samples from the time domain to a domain where the jamming component affects a limited number of samples and the interference can be considered sparse. This transform is applied to the snapshot samples $y[n]$ before correlation as $Y[k] = \mathbf{T}_1(y[n])$, where index k refers to the set of discrete frequencies. The selected ZMNL, denoted as $\psi(\cdot)$, is the Huber's non-linearity, which reduces the impact of interfered samples in the transformed domain and can be defined as (Wang and Poor, 1999)

$$\psi_H(Y[k]) = \begin{cases} Y[k] & \text{for } |Y[k]| \leq T_h \\ T_h \text{ csign}(Y[k]) & \text{for } |Y[k]| > T_h \end{cases} , \tag{4}$$

where $|\cdot|$ is the absolute value operator, T_h is a decision threshold with an optimal value of 1.345σ (Fox, 2002) and csign$(\cdot)$ can be defined as

$$\text{csign}(Y[k]) = \begin{cases} \frac{Y[k]}{|Y[k]|} & \text{for } Y[k] \neq 0 \\ 0 & \text{for } Y[k] = 0 \end{cases} . \tag{5}$$

$\mathbf{T}_2$ inverts the effects of $\mathbf{T}_1$ and brings back the samples from the transformed domain to the initial one, i.e. the time domain, as $\tilde{y}[n] = \mathbf{T}_2(Y_\psi[k])$. When RIM is applied in the time domain, $\mathbf{T}_1$ is a low pass-filter and $\mathbf{T}_2$ is the identity operator. When applied in the frequency domain, $\mathbf{T}_1$ and $\mathbf{T}_2$ can be computed as the Fast Fouriter Transform (FFT) and the Inverse Fast Fourier Transform (IFFT), respectively. The impact of the interference signal $i[n]$ on the RIM output clean samples $\tilde{y}[n]$ has been reduced. After this, a standard receiver architecture is adopted using $\tilde{y}[n]$ instead of the initial snapshot samples $y[n]$. The robust Cross Ambiguity Function (CAF) is computed as (Borio, 2017a)

$$\mathcal{C}_\psi(\tau, f_d) = \sum_{n=0}^{N-1} \tilde{y}[n] c\left(nT_s - \tau\right) e^{-j2\pi f_d n T_s} , \tag{6}$$

where the satellite index was omitted for simplicity.

1. Loss of Efficiency

The LoE given by Huber's non-linearity is evaluated in Borio et al. (2018). It is defined as the performance degradation caused by the non-linearity in the absence of interference and it is given by the ratio

$$L_0(T_h) = \frac{\text{SNR}_{\text{out}}^{\psi}}{\text{SNR}_{\text{out}}} , \tag{7}$$

where SNR_{out} corresponds to the post-correlation signal-to-noise ratio (SNR) given by $\mathcal{C}(\tau, f_d)$, and $\text{SNR}_{\text{out}}^{\psi}$ corresponds to the post-correlation SNR given by $\mathcal{C}_\psi(\tau, f_d)$. The quality of the CAF can be measured with the post-correlation SNR as (Betz,

2000, 2001; Borio et al., 2018)

$$\text{SNR}_{\text{out}} = \max_{\tau, f_d} \frac{|\mathbb{E}\{\mathcal{C}(\tau,\ f_d)\}|^2}{\frac{1}{2}\text{Var}\{\mathcal{C}(\tau,\ f_d)\}}\ . \tag{8}$$

Results in Borio et al. (2018) show that the LoE values are the same for both time and frequency domain processing, with a maximum value of 1.05 dB. The dual-domain RIM (or DD-RIM) is proposed in Li et al. (2019) and consists in sequentially applying the RIM algorithm in the time and frequency domains. This approach exploits the sparsity of the jamming signals in both domains with the cost of a duplicated LoE.

2. Median Absolute Deviation

The value of the snapshot variance is required for the calculation of the Huber's non-linearity threshold T_h, which depends on σ^2. The median absolute deviation (MAD) is a robust measure of statistical dispersion that can be computed as

$$\text{MAD}(\mathbf{x}) = \beta\ \text{Med}(|\mathbf{x} - \text{Med}(\mathbf{x})|), \tag{9}$$

being $|\cdot|$ the absolute value operator, Med($\mathbf{x}$) the median of $\mathbf{x}$, and β a constant scale factor. This method is widely used due to its simplicity, featuring a breakdown point of 0.5 (Rousseeuw and Croux, 1993). It may be used as an asymptotically consistent estimator to estimate the standard deviation σ. The value of the scale factor β is distribution-dependent, being set to $\beta = 1.4815$ in the case of Gaussian distributions.

When applying RIM in the frequency domain, frequency samples are used for variance estimation, with the Huber's non-linearity threshold T_h set to its optimal value of 1.345σ (Fox, 2002). To improve robustness, the variance is estimated recursively as

$$\bar{\sigma}^2_m = \frac{\sigma^2_m}{m} + \frac{m-1}{m}\bar{\sigma}^2_{m-1}\ , \tag{10}$$

where m is the index of the recursive iteration and $\bar{\cdot}$ is defined as the recursive operator. Therefore, $\bar{\sigma}^2_m$ corresponds to the recursive MAD variance estimation at update m and is dependent on the recursive estimation at update $m-1$, $\bar{\sigma}^2_{m-1}$. The recursive update at any time instant is identical to non-recursively averaging all points up to that time.

IV. EXPERIMENTAL SETUP

1. Signal Generation

GPS L1, Galileo L1 and Beidou B1 signals are generated with a sampling frequency equal to the receiver bandwidth (i.e., 4.5 MHz). Quantization is applied to the output of the simulation tool. The RIM algorithm performance is assessed with 2, 4 and 8 quantization bits and an adaptive quantization dynamic range that is proportional to the snapshot variance, which increases with the presence of jamming. For large dynamic ranges, a higher resolution is needed to perceive the contribution of useful GNSS signal. This can be achieved by increasing the number of quantization bits. The AGC optimal gain factor values are calculated as shown in Table 1. At this stage, σ^2 corresponds to the snapshot variance calculated without recursion or robustness.

The baseband signal models used for interference simulation are presented in Table 2, which considers the classification criteria from Morales Ferre et al. (2019). Jammer 1 is a single-tone CW with f_J set to -1 kHz with respect to the baseband frequency, jammer 2 is a chirp interference sweeping the whole receiver bandwidth ($f_{\text{min}} = -\frac{f_s}{2}$ and $f_{\text{max}} = \frac{f_s}{2}$), and jammer 3 is a wideband jammer with a sweep range of 20 MHz (from -10 to 10 MHz). Both jammers 2 and 3 have a sweep period of duration $T_{\text{sweep}} = 10\ \mu s$. Figure 1 shows spectrogram plots of a clean 120 ms snapshot interfered by jammers 1, 2 and 3. With $f_s = 4.5$ MHz and $T_{\text{sweep}} = 10\ \mu s$, the number of samples per sweep period is 45, which leads to a poor spectrogram resolution. We thereupon selected a higher sweep period of $T_{\text{sweep}} = 0.06$ for spectrogram generation. The spectrogram of jammer 1 shows a constant tone centered at $f_J = -1$ kHz, while the whole receiver bandwidth is swept in the cases of jammers 2 and 3. Wideband interferences with a sweep range higher than the receiver bandwidth can be interpreted as pulsed interferences, as the receiver is only affected by the jamming attack during the time when $f_J(j)$ is within the receiver bandwidth. This is the case of jammer 3, whose bandwidth (20 MHz) is larger than the receiver bandwidth (4.5 MHz) and consequently is seen as a pulsed interference in the time domain despite its signal model being the one of chirps and therefore being grouped into Class II. This pulsed effect can be clearly observed in Figure 1c, where there is no jamming effect for $t \in [35,\ 85]$ ms approximately, given that the jammer is attacking frequencies outside the receiver bandwidth during that time period. On the other hand, jammer 2 attacks frequencies within the receiver bandwidth for $t = [0,\ 120]$ ms, i.e., the whole snapshot. The three jammers behave as outliers in the frequency domain and only jammer 3 behaves as an outlier in the time domain, given its pulsed effect. Considering this, the RIM algorithm is only applied in the frequency domain throughout this paper, as applying it in the time domain with dual-domain RIM would only help in the case of jammer 3 with the cost of duplicating the LoE. The lines in the spectrogram

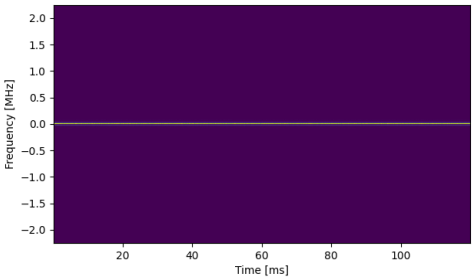

(a) Spectrogram with jammer 1

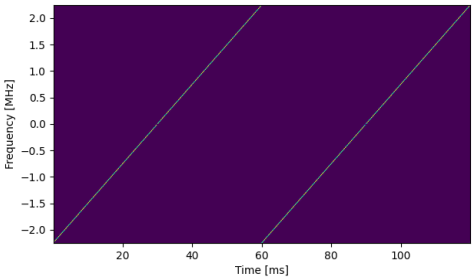

(b) Spectrogram with jammer 2

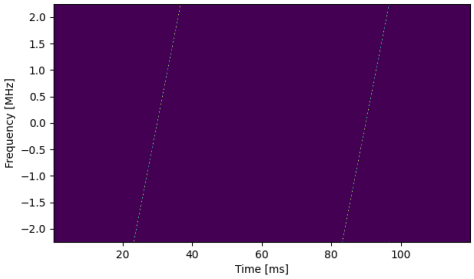

(c) Spectrogram with jammer 3

Figure 1: Baseband model spectrograms of simulated GPS L1 signal interfered by jammers 1, 2 and 3, with C/N_0 = 45 dB and J/N = 15 dB.

from Figure 1c are difficult to see because the power of jammer 3 does not overcome the GNSS signal power as much as jammers 1 and 2. Given that jammer 3 is spread over a larger bandwidth, it may be considered to be a wideband interference when compared to jammer 2, for instance.

ID	Class	Type	Baseband model	Design parameters
1	I	CW	$i[n] = A_J \exp(j2\pi f_J n T_s)$	A_J, f_J
2	II	Chirp	$i[n] = A_J \exp(j2\pi T_s \sum_{j=0}^{n} f_J[j])$ (11)	A_J, T_{sweep}, Δf
3	II	Pulsed Chirp	Equation (11) with $\Delta f > B_{R_x}$	A_J, T_{sweep}, Δf

Table 2: Classification of the implemented jamming baseband signal models, according to Morales Ferre et al. (2019).

By characterizing mass-market jammers in previous literature (Borio et al., 2013), it has been shown that the maximum jamming transmission peak power typically varies from -10 to 30 dBm. This corresponds to approximately 95 to 130 dB of J/N ratio in the case of our receiver. To do the conversion from J/N to J/N_0 (see Equation 3), the receiver bandwidth B_{R_x} is considered to be equal to the sampling frequency $f_s = 4.5$ MHz, as we are performing complex sampling. Path loss attenuation plays a role in the actual J/N ratio value observed at the receiver. To consider the worst-case scenario, in which the jammer suffers from the least possible attenuation, the free-space path loss (FSPL) factor is computed as FSPL $= \left(\frac{4\pi d}{\lambda}\right)^2$, where d corresponds to the jammer-receiver distance and λ corresponds to the signal wavelength, which depends on the frequency of transmission. As L-band wavelengths have values between 15 and 30 cm, the worst-case scenario (i.e., least path-loss attenuation for the jammer) is given by $\lambda = 30$ cm, resulting in 60 dB for $d = 100$ m. Considering that the maximum jammer transmitted peak power can reach a value of 130 dB, the maximum J/N ratio that a receiver will experience is 70 dB for $d = 100$ m. Consequently, the range of J/N ratio values that are selected to assess the performance of the RIM algorithm varies from 0 to 95 dB, where additional 25 dB have been considered as a safety margin.

2. System Model

A diagram of the system model is presented in Figure 2, where $r[n]$ corresponds to the clean snapshot generated by the GNSS signal simulator and $i[n]$ is the jamming interference generated as explained in the previous subsection. The anti-jamming module is located between the simulation tool, which is equivalent to the system front end, and the baseband processing block. J and M stand for *jammer* and *mitigation* and indicate whether these two are enabled, resulting in four possible configurations. If $J = 1$, the output of the simulation tool is polluted by the jammer as $y[n] = r[n] + i[n]$, while $y[n] = r[n]$ if $J = 0$. If $M = 1$, the RIM algorithm is applied to the output signal of the simulator tool $y[n]$. In this case, the input of the baseband processing block is $\tilde{y}[n]$, where $\tilde{\cdot}$ indicates the impact of the front-end filtering. If $M = 0$, the input signal of the baseband processing block is $y[n]$.

When applying the RIM algorithm in the frequency domain, the Huber's non-linearity is applied to the snapshot FFT samples, which must be normalized by $\sqrt{N_{\text{snap}}}$. The algorithm is applied every 1 ms instead of to all snapshot samples. This is because the range of spectrum affected by the interference is proportional to the considered number of samples. The smaller the affected range, the easier it is to see the interference as an outlier. Also, the computational cost given by the FFT and IFFT operations is proportional to $N \log(N)$, being N the number of FFT samples. Consequently, it is more efficient to divide the snapshot into small intervals. the MAD variance estimation is computed every 1 ms. This means that 4500 samples are used for each recursive update.

Each case of study within Experiment 1 is defined by a value of J, M and a jammer type. For each case of study, 10 snapshots of 120 ms (i.e., 1200 ms of recording) are processed. For the LoE assessment, two snapshots of 120 ms (i.e. 240 ms of recording) are processed. The effect of signal quantization is studied for 2, 4 and 8 quantization bits.

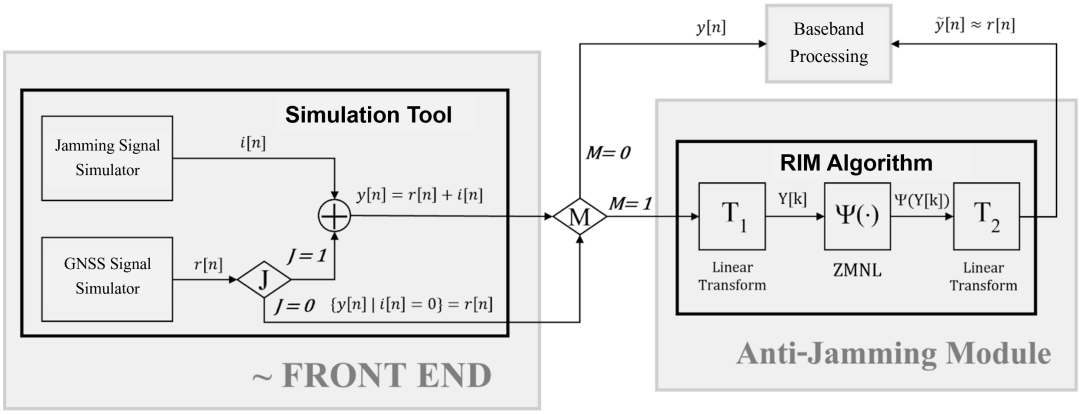

Figure 2: Diagram of the system model in Experiment 1. J and M stand for *jammer* and *mitigation* and indicate whether these two are enabled.

V. RESULTS

This section aims to assess how changes in signal quantization affect the robustness of the snapshot receiver against jamming interferences, both when the RIM algorithm is disabled and enabled. When the RIM algorithm is disabled, we study how the jammer power measured at the receiver and the waveform of an interfered signal are affected by a low number of quantization bits, which we denote as B. When enabling the RIM algorithm, we study whether the gain it provides is proportional to B. An analysis of the algorithm performance under several configurations allows us to decide whether this mitigation technique can bring enough robustness to a snapshot receiver.

The monitored metrics to assess the RIM algorithm performance are the C/N_0, PVT availability and the number of visible satellite vehicles (SVs) after the acquisition stage. The attenuation in GNSS signal as a consequence of jamming interference can be extracted from the C/N_0 ratio as a function of the J/N ratio. C/N_0 ratios lower than 30 dB are considered to be low because they require a high-sensitivity receiver to obtain reasonable positioning accuracy. A PVT solution is considered to be valid if it passes the receiver integrity test.

1. Effect of Signal Quantization

a) Effective J/N

As explained in Section II.2, snapshot samples affected by jamming suffer from a clipping effect when the number of quantization bits is low. In these cases, the number of different quantization values is not enough to allow for a proper signal representation. Consequently, the J/N observed at the receiver, which we refer to as the *effective* J/N, differs from the actual J/N value. In Figure 4a, the value of effective J/N observed at the receiver is studied as a function of the actual value of J/N used to simulate the jamming signal, which is a known input parameter of the interference simulator. This figure shows that the quantization dynamic range increases proportionally to B and that a saturation point occurs when the whole dynamic range is used. When this happens, an increase in the jamming power cannot be further perceived by the receiver. The saturation point occurs at 0, 12, 17 and 35 dB of J/N with values of approximately 0, 5, 12 and 33 dB of effective J/N for 1, 2, 4 and 8 quantization bits. This means that, for instance, in the case of $B = 4$, the value of J/N measured at the receiver cannot be greater than 12 dB, and this value is reached when the J/N of the simulated interference is 17 dB. For a low B, the magnitude of J/N that the receiver can perceive is also low, which can actually benefit the receiver performance when no anti-jamming technique is available. For $B = 2$, we do not have enough resolution to characterize an interference, which leads to poor results when applying anti-jamming techniques. Nevertheless, as quantization values are limited, and signal power is more spread due to waveform distortion, the effective J/N at the receiver is very low, which diminishes the effect of powerful interference without the need for mitigation.

b) Waveform Distortion

Figure 4a shows how for $B = 8$ and before saturation, effective J/N values coincide with the actual J/N used for interference simulation. On the other hand, this does not happen for lower values of B. We believe that this happens due to the waveform distortion introduced by a low number of quantization bits, which causes artifacts taking the form of multiple frequency harmonics in the signal spectra. This phenomenon is evidenced by the results presented in Figure 3, where PSD and spectrogram figures of jammer 1 are shown for $B = \{2,\ 4,\ 8\}$. The interference waveform strongly differs from the baseband signal model in Table 2 when quantizing with a low number of bits ($B < 8$). Also, in the case of $B = \{2,\ 4\}$, the power is spread across multiple frequencies, differing from the single-tone obtained for $B = 8$. From now on, we use the J/N ratio to refer exclusively to the value used to simulate the jamming interferences.

c) Quantization Gain

In Figure 4b, the performance of the RIM algorithm is assessed under the presence of jammer 1 as a function of the J/N ratio for $B = \{2,\ 4,\ 8\}$. The performance metric in this figure is the number of visible SVs. Results are presented both when RIM is enabled and disabled. A gain of 10, 20 and 35 dB is observed when applying the RIM algorithm for 2, 4 and 8 quantization bits. This suggests that the gain obtained when applying the RIM algorithm is proportional to the number of quantization bits. Consequently, although the baseline performance can be better for $B = 2$ when RIM is not applied, the gain provided by the anti-jamming algorithm increases with greater values of B, thus providing an actual protection against jamming attacks.

Considering the results presented in this section, it can be stated that when the RIM algorithm is not applied, the receiver is more robust in terms of number of visible SVs and PVT availability when quantizing with a low number of bits. However, receiver performance in that case is not desirable. Therefore, it is necessary to apply a mitigation algorithm such as RIM to obtain a gain that is proportional to the number of quantization bits.

2. Robust Interference Mitigation

a) Algorithm Performance

An assessment of the RIM algorithm in the frequency domain for $B = \{2,\ 4,\ 8\}$ is presented in Figures 5a, 5b and 6, respectively. The performance metrics under study are the number of visible SVs, PVT availability, and the average C/N_0. C/N_0 values are plotted only when the receiver passes the integrity test.

In the case of jammer 1 and without applying RIM, PVT availability falls to 0 at 30 dB of J/N ratio for $B = \{4,\ 8\}$. With $B = 2$, the receiver is more robust to this interference in terms of PVT availability, as it falls to 0 at 40 dB of J/N. The same result is observed regarding the number of visible SVs, as this metric falls to 0 at 30 dB of J/N ratio for $B = \{4,\ 8\}$ and at 45 dB for $B = 2$. When mitigation is enabled, there is a gain of 15, 20 and 35 dB for $B = \{2,\ 4,\ 8\}$, respectively. This gain, and therefore the receiver performance, is proportional to the number of quantization bits when anti-jamming can be applied. A clear improvement in the average C/N_0 values can be observed when increasing B. The gain in this metric is of approximately 5, 10 and 30 dB for $B = \{2,\ 4,\ 8\}$.

When it comes to jammer 2, without applying RIM and in terms of PVT availability and number of visible SVs, the receiver is also $5-10$ dB more resistant for $B = 2$. However, these two metrics fall to 0 at approximately $J/N = 20$ dB for $B = \{2,\ 4,\ 8\}$, which is very soon. This is why it is required to enable the RIM algorithm, which makes it possible to acquire all the satellites

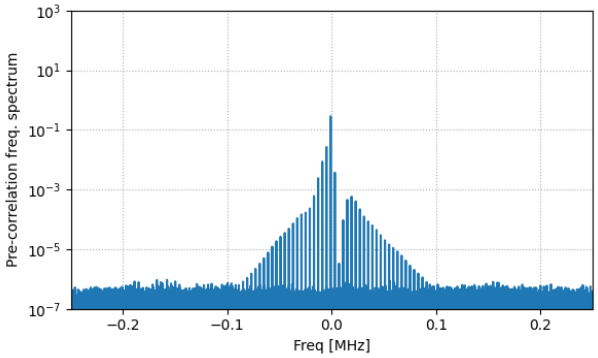

(a) PSD of jammer 1 with $B = 2$

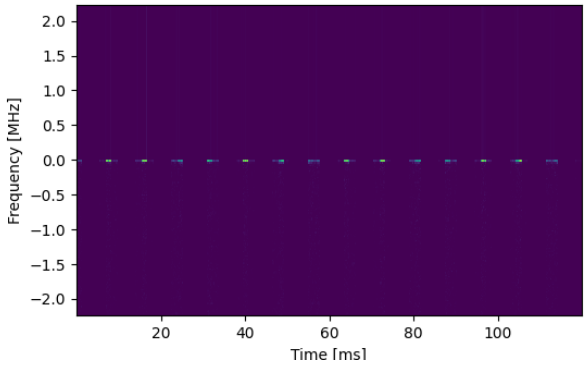

(b) Spectrogram of jammer 1 with $B = 2$

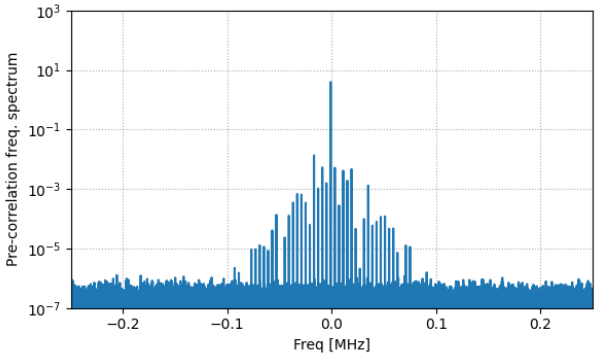

(c) PSD of jammer 1 with $B = 4$

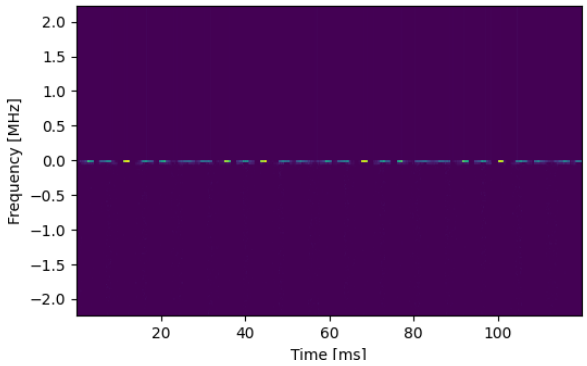

(d) Spectrogram of jammer 1 with $B = 4$

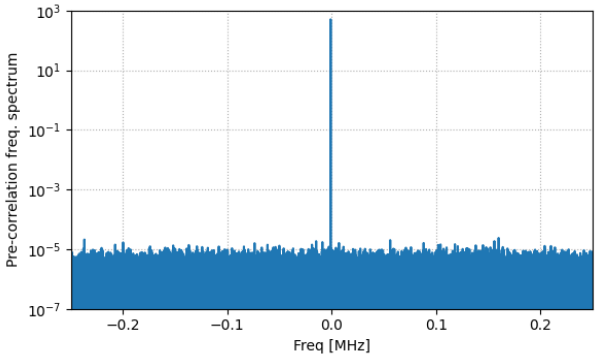

(e) PSD of jammer 1 with $B = 8$

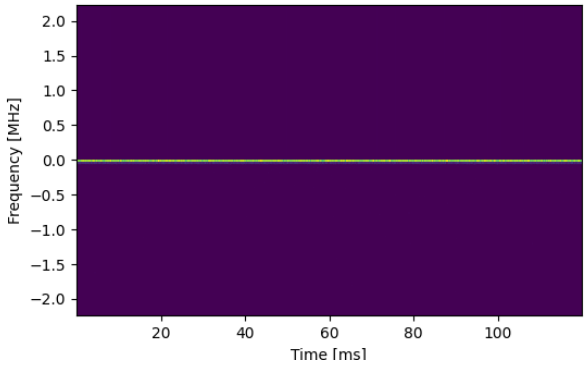

(f) Spectrogram of jammer 1 with $B = 8$

Figure 3: Spectra and spectrograms (in the baseband) of 120 ms of simulated GPS L1, GAL E1 and BDS B1 signals interfered by jammer 1 for 2, 4 and 8 quantization bits. C/N_0 is 45 dB and J/N is 30 dB.

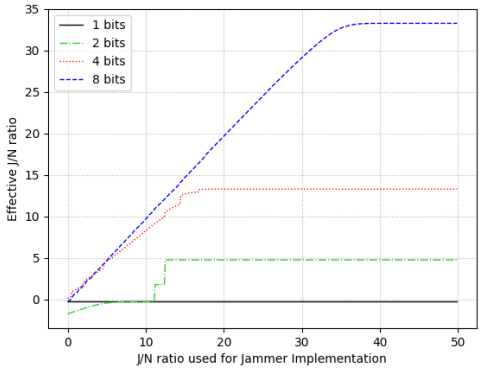

(a) Evolution of the J/N ratio effective value at the receiver for different quantization bits.

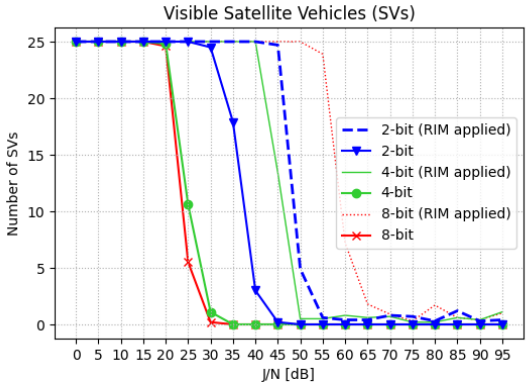

(b) Performance of the RIM algorithm under the attack of jammer 1 (CW) with 2, 4 and 8 quantization bits.

Figure 4: Effect of Signal Quantization.

for $B = \{2,\ 4,\ 8\}$ and all tested jammer powers. A similar gain in the average C/N_0 as the one with jammer 1 is observed for this interference.

As jammer 3 behaves as an outlier in the time domain, and due to the clipping effect mentioned in Section II.2, with $B = 2$ all satellites are acquired even when mitigation is disabled. With higher number of quantization bits, the performance of the receiver starts dropping at 20 dB of J/N ratio. However, the RIM algorithm is able to mitigate jammer 3 under all the assessed values of J/N ratio. When mitigation is not applied, average C/N_0 values are higher with 2 quantization bits, which is due to the effective J/N ratio saturation effect explained in the previous subsection. Also, average C/N_0 results are the same for 4 and 8 quantization bits. When applying the RIM algorithm, a gain proportional to the number of quantization bits can be observed in the average C/N_0.

b) Efficiency Analysis

The measured LoE introduced by the frequency RIM with MAD variance estimation applied every 1 ms is 0.45, 0.48 and 0.49 dB for $B = \{2,\ 4,\ 8\}$ when averaging each satellite LoE. This corresponds to a difference of approximately 0.15 dB with respect to the theoretical value (Borio et al., 2018). This difference is not considered a potential issue for satellite acquisition.

VI. CONCLUSION

In this paper, the performance of the robust interference mitigation (RIM) algorithm for interference mitigation has been assessed in the context of a GNSS snapshot receiver. Different levels of quantization were investigated, namely 2, 4 and 8 quantization bits, under the presence of three different jamming interferences. These interferences were simulated as representative cases of common mass-market jammer characteristics. A study on the effect of signal quantization in GNSS snapshot receivers in the context of interference mitigation is provided, suggesting that signal quantization has a multifaceted effect, such as the effective J/N observed at the receiver, the signal waveform and the robustness provided by the RIM algorithm. When the RIM algorithm is not applied, the receiver is more robust in terms of some metrics (e.g., number of visible SVs and PVT availability) when quantizing with a low number of bits, although its performance is not desirable. This is explained by a clipping of the interference, which brings inherent robustness (similarly to a pulse blanking method). However, when applying the RIM algorithm, the obtained gain improves with the number of quantization bits. Hence, a high number of quantization bits is preferred to benefit from the assistance provided by the implemented mitigation technique. This finding is consistent with the literature since higher bit levels facilitate the interference reconstruction and mitigation. Results suggest that applying the RIM algorithm in the frequency domain is sufficient to mitigate interferences in typical environments, as most interferences behave as outliers in the frequency domain. A clear improvement in receiver performance is observed when increasing the number of quantization bits, in terms of the number of visible SVs, PVT availability and average C/N_0.

ACKNOWLEDGEMENTS

This work has been partially supported by the ESA NAVISP Programme under activity NAVISP-EL2-096, and by the NSF under Awards ECCS-1845833 and CCF-2326559.

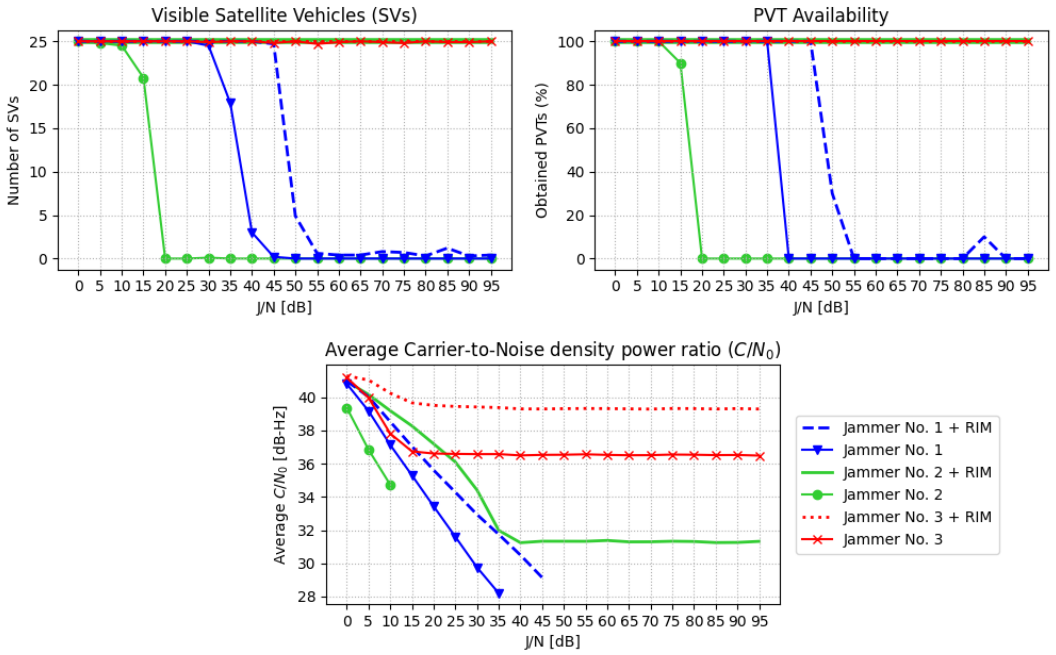

(a) $B = 2$

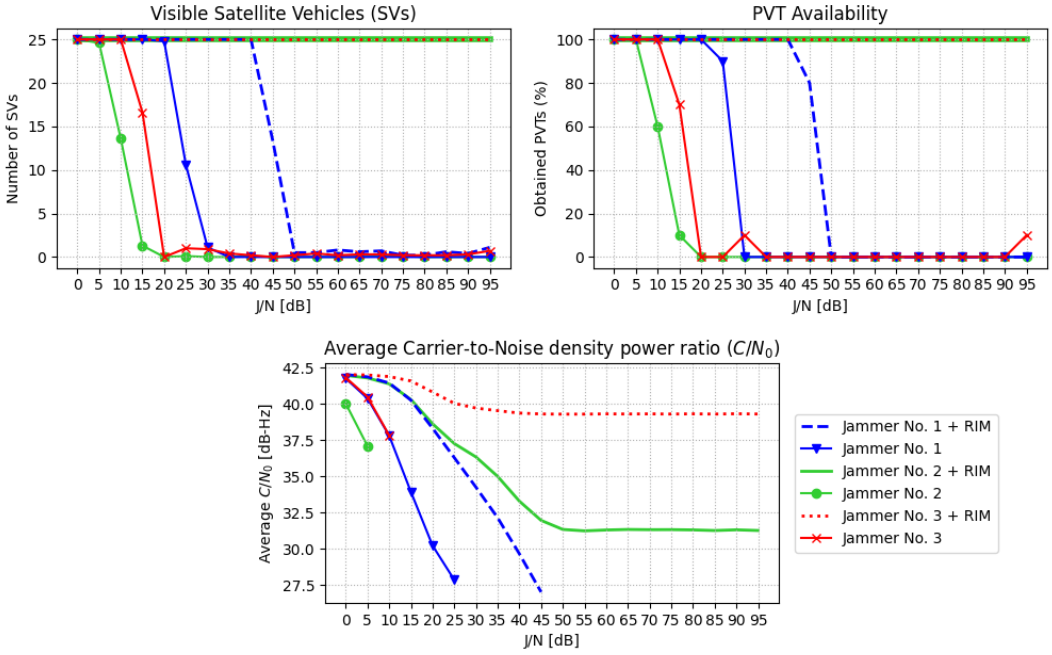

(b) $B = 4$

Figure 5: Assessment of the frequency RIM algorithm for 2 and 4 quantization bits. The performance metrics under study are the number of visible SVs, PVT availability and average C/N_0.

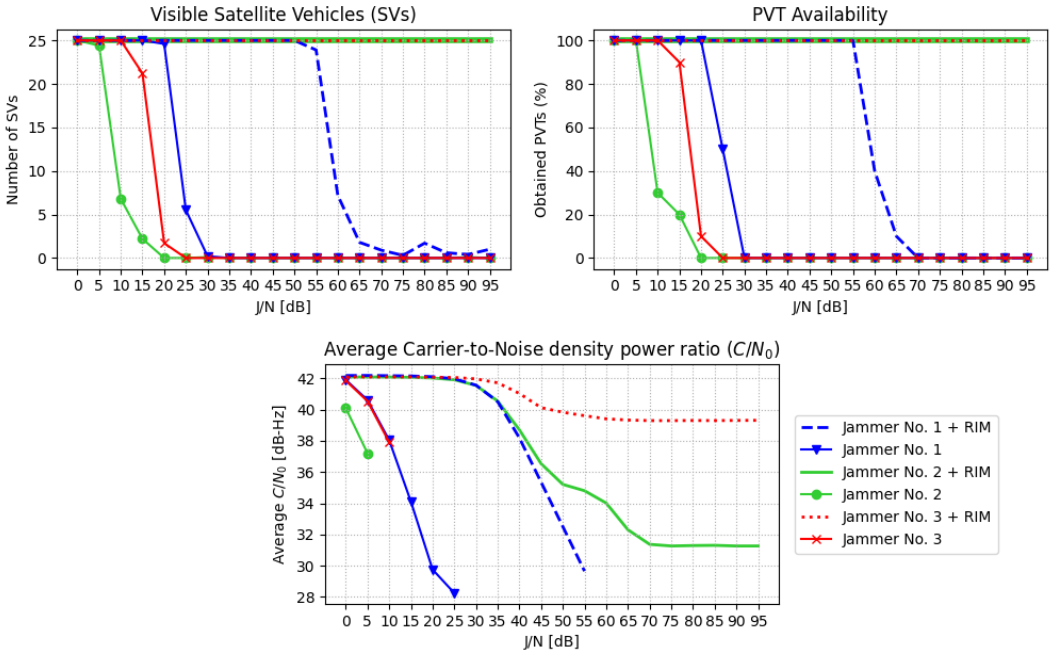

Figure 6: Assessment of the frequency RIM algorithm for 8 quantization bits.

REFERENCES

Amin, M. G., Closas, P., Broumandan, A., and Volakis, J. L. (2016a). Vulnerabilities, threats, and authentication in satellite-based navigation systems. In *Proceedings of the IEEE*, volume 104, pages 1169–1173.

Amin, M. G., Wang, X., Zhang, Y. D., Ahmad, F., and Aboutanios, E. (2016b). Sparse arrays and sampling for interference mitigation and DOA estimation in GNSS. In *Proceedings of the IEEE*, volume 104, pages 1302–1317.

Betz, J. W. (2000). Effect of Narrowband Interference on GPS Code Tracking Accuracy. In *Proceedings of the 2000 National Technical Meeting of The Institute of Navigation*, pages 16–27, Anaheim, CA, US.

Betz, J. W. (2001). Effect of Partial-Band Interference on Receiver Estimation of C/N_0: Theory. In *Proceedings of the 2001 National Technical Meeting of The Institute of Navigation*, pages 817–828, Long Beach, CA, USA.

Borio, D. (2008). *A statistical theory for GNSS signal acquisition*. PhD thesis, Politecnico di Torino.

Borio, D. (2016). Swept GNSS jamming mitigation through pulse blanking. In *2016 European Navigation Conference (ENC)*, pages 1–8, Helsinki, Finland.

Borio, D. (2017a). Myriad Non-Linearity for GNSS Robust Signal Processing. *IET Radar, Sonar & Navigation*, 11(10):1467–1476.

Borio, D. (2017b). Robust signal processing for GNSS. In *2017 European Navigation Conference (ENC)*, pages 150–158, Lausanne, Switzerland.

Borio, D. and Closas, P. (2017). A Fresh Look at GNSS Anti-Jamming. *Inside GNSS*, 12:54–61.

Borio, D., Dovis, F., Kuusniemi, H., and Presti, L. L. (2016). Impact and detection of GNSS jammers on consumer grade satellite navigation receivers. In *Proceedings of the IEEE*, volume 104, pages 1233–1245.

Borio, D., Fortuny, J., and O'Driscoll, C. (2013). Spectral and Spatial Characterization of GNSS Jammers. In *Proceedings of the 7th GNSS Vulnerabilities and Solutions Conference*, pages 1–17, Baska, Croatia.

Borio, D., Li, H., and Closas, P. (2018). Huber's non-linearity for GNSS interference mitigation. *Sensors*, 18(7):2217.

Borio, D., O'Driscoll, C., and Fortuny, J. (2012). GNSS Jammers: Effects and countermeasures. In *Proceedings of the 6th ESA Workshop on Satellite Navigation Technologies and European Workshop on GNSS Signals and Signal Processing*, pages 1–7, Noordwijk, Netherlands.

Díez-García, R. and Camps, A. (2019). Impact of signal quantization on the performance of RFI mitigation algorithms. *Remote Sensing*, 11(17):2023.

Dumitraschkewitz, P. (2020). *GNSS snapshot techniques for quality of service monitoring*. PhD thesis, Graz University of Technology.

Fernández-Hernández, I. and Borre, K. (2016). Snapshot positioning without initial information. *GPS Solutions*, 20:605–616.

Fernández-Prades, C., Arribas, J., and Closas, P. (2016). Robust GNSS Receivers by Array Signal Processing: Theory and Implementation. In *Proceedings of the IEEE*, volume 104, pages 1207–1220.

Fox, J. (2002). *An R and S-Plus Companion to Applied Regression*. Sage Publications, CA, US.

Gao, G. X., Sgammini, M., Lu, M., and Kubo, N. (2016). Protecting GNSS Receivers From Jamming and Interference. In *Proceedings of the IEEE*, volume 104, pages 1327–1338.

Garcia-Molina, J. A. and Crisci, M. (2016). Snapshot localisation of multiple jammers based on receivers of opportunity. In *Proceedings of the 8th ESA Workshop on Satellite Navigation Technologies and European Workshop on GNSS Signals and Signal Processing*, pages 1–6, Noordwijk, Netherlands.

Kaplan, E. D. and Hegarty, C. (2005). *Understanding GPS/GNSS: Principles and Applications*. Artech House Publishers, Norwood, MA, USA, 3rd edition.

Li, H., Borio, D., and Closas, P. (2019). Dual-domain robust GNSS interference mitigation. In *Proceedings of the 32nd International Technical Meeting of the Satellite Division of The Institute of Navigation (ION GNSS+)*, pages 991–1002, Miami, FL, US.

Linty, N. (2015). *Snapshot Estimation Algorithms for GNSS Mass-Market Receivers*. PhD thesis, Politecnico di Torino.

Liu, X., Ribot, M., Gusi-Amigó, A., Closas, P., Rovira-Garcia, A., and Sanz, J. (2020). RTK Feasibility Analysis for GNSS Snapshot Positioning. In *Proceedings of the 33rd International Technical Meeting of the Satellite Division of The Institute of Navigation (ION GNSS+)*, pages 2911–2921.

Liu, X., Ribot, M. Á., Gusi-Amigó, A., Rovira-Garcia, A., Sanz, J., and Closas, P. (2021). Cloud-based single-frequency snapshot RTK positioning. *Sensors*, 21(11):3688.

Medina, D., Lass, C., Marcos, E. P., Ziebold, R., Closas, P., and García, J. (2019a). On GNSS Jamming Threat from the Maritime Navigation Perspective. In *2019 22th International Conference on Information Fusion (FUSION)*, pages 1–7, Ottawa, ON, Canada.

Medina, D., Li, H., Vilà-Valls, J., and Closas, P. (2019b). Robust Statistics for GNSS Positioning under Harsh Conditions: A Useful Tool? *Sensors*, 19(24):5402.

Mitch, R. H. et al. (2011). Signal characteristics of civil GPS jammers. In *Proceedings of the 24th International Technical Meeting of the Satellite Division of The Institute of Navigation*, pages 1907–1919, Portland, OR, US.

Mitch, R. H., Psiaki, M. L., Powell, S. P., and O'Hanlon, B. W. (2013). Signal acquisition and tracking of chirp-style GPS jammers. In *Proceedings of the 26th International Technical Meeting of the Satellite Division of The Institute of Navigation (ION GNSS+)*, pages 2893–2909, Nashville, TN, US.

Morales Ferre, R., De La Fuente, A., and Simona Lohan, E. (2019). Jammer classification in GNSS bands via machine learning algorithms. *Sensors*, 19(22):4841.

Morales Ferre, R., Richter, P., Falletti, E., De La Fuente, A., and Simona Lohan, E. (2020). A Survey on Coping With Intentional Interference in Satellite Navigation for Manned and Unmanned Aircraft. In *IEEE Communications Surveys & Tutorials*, volume 22, pages 249–291.

Pullen, S. and Gao, G. (2012). GNSS jamming in the name of privacy: Potential threat to GPS aviation. *Inside GNSS*, 7(2):33–43.

Rousseeuw, P. J. and Croux, C. (1993). Alternatives to the median absolute deviation. *Journal of the American Statistical Association*, 88(424):1273–1283.

Wang, X. and Poor, H. V. (1999). Robust multiuser detection in non-Gaussian channels. *IEEE Transactions on Signal Processing*, 47(2):289–305.

Wu, P., Calatrava, H., Imbiriba, T., and Closas, P. (2023). Jammer classification with Federated Learning. In *2023 IEEE/ION Position, Location and Navigation Symposium (PLANS)*, pages 228–234, Monterey, CA, US.